Journal of Inflammation Research

Dovepress
Taylor & Francis Group

Open Access Full Text Article

ORIGINAL RESEARCH

Integrating Gut Microbiome and Metabolomics with Magnetic Resonance Enterography to Advance Bowel Damage Prediction in Crohn's Disease

Lili Huang[1,*], Jixin Meng[1,2,*], Shaochun Lin[1,*], Zhenpeng Peng[1,*], Ruonan Zhang[1], Xiaodi Shen[1], Weikai Zheng[1], Qingzhu Zheng[1], Luyao Wu[1], Xinyue Wang[1], Yangdi Wang[1], Ren Mao[3], Canhui Sun[1], Xuehua Li[1], Shi-Ting Feng[1]

[1]Department of Radiology, The First Affiliated Hospital, Sun Yat-Sen University, Guangzhou, People's Republic of China; [2]Department of Radiology, Henan Provincial People's Hospital & Zhengzhou University People's Hospital, Zhengzhou, People's Republic of China; [3]Department of Gastroenterology, The First Affiliated Hospital, Sun Yat-Sen University, Guangzhou, People's Republic of China

*These authors contributed equally to this work

Correspondence: Xuehua Li; Shi-Ting Feng, Department of Radiology, The First Affiliated Hospital, Sun Yat-Sen University, Guangzhou, People's Republic of China, Tel +86-20-87755766-8471, Fax +86-20-87615805, Email lxueh@mail.sysu.edu.cn; fengsht@mail.sysu.edu.cn

Purpose: Cumulative bowel damage (BD) critically influences the progression and prognosis of Crohn's disease (CD). Although the Lémann Index (LI) remains the standard for BD assessment, its clinical utility is limited by heavy reliance on extensive clinical data. Multiparametric magnetic resonance enterography (MRE) provides noninvasive macroscopic evaluation of BD severity, however, it fails to characterize microscopic alterations. We therefore integrated MRE with gut microbiome and metabolomic data to uncover mechanistic insights and develop a comprehensive model for better prediction of BD.

Methods and Results: In this prospective two-center study, 309 CD patients were stratified into BD and non-BD groups using LI. Patients underwent MRE, fecal 16S rRNA gene sequencing, and fecal/serum metabolomic analysis. Thirty healthy controls were included for comparison. The relationships between microbial/metabolic factors and MRE features were explored using correlation and mediation analyses. Seven machine learning algorithms, each paired with seven distinct combinations of multi-omics features, were evaluated using nested 5-fold cross-validation to construct an optimal prediction model. BD patients exhibited reduced gut microbial diversity ($P<0.05$), with *Erysipelatoclostridium* and *[Ruminococcus]_gnavus_group* as key discriminators. Metabolomics revealed elevated fecal aromatic amino acids and depleted serum glycerophospholipids/sphingolipids ($P<0.05$) linked to MRE-quantified features through mediation by microbial pathways (eg, 22.8% mediation effect of *Prevotella_9* on penetration, $P_{ACME}=0.022$). The optimal Xtreme Gradient Boosting Classifier (XGBC) model integrating three microbial genera, six fecal metabolites, three serum metabolites, and three MRE features achieved superior performance (AUC 0.857 and 0.829 in the derivation and external validation cohorts, respectively). SHapley Additive exPlanations (SHAP) analysis prioritized perianal diseases, *Erysipelatoclostridium*, and fecal alanine as key contributors.

Conclusion: Our study underscores the interplay between gut microbial dysbiosis, metabolic alterations, and MRE-quantified structural changes in BD patients. The integrated multi-omics model provides a promising tool for BD prediction, enabling precise CD severity stratification and personalized clinical decision-making.

Plain Language Summary: Crohn's disease is a long-term condition that causes inflammation of the digestive tract and can lead to significant bowel damage over time. Although tools such as the Lémann Index help assess this damage, they mainly rely on clinical records and do not reveal the biological processes behind the damage. In this study, we aimed to develop a more accurate method for predicting bowel damage. We combined the three methods into a single comprehensive test.

- **Imaging**: Magnetic resonance enterography (MRE), a noninvasive scan, was used to capture clear images of the bowel. This allowed us to observe signs of inflammation, such as thickened bowel walls, swelling in the surrounding tissues, abnormal blood vessel patterns, as well as other structural damage.
- **Gut Bacteria Analysis**: We examined stool samples to understand the variety and balance of the gut bacteria.

Received: 25 February 2025
Accepted: 28 May 2025
Published: 11 June 2025

- **Metabolite Testing**: We analyzed both stool and blood samples to measure metabolic markers.

We studied 309 individuals with Crohn's disease and compared them with 30 healthy volunteers. Our findings revealed that the changes seen on MRE were closely linked to shifts in gut bacteria and metabolic markers. For instance, individuals with bowel damage had less diverse gut bacteria, higher levels of certain amino acids in their stool, and lower levels of important lipids in their blood.

These results suggest that integrating these tests into a single diagnostic tool could help doctors quickly and accurately identify bowel damage. This, in turn, may lead to more personalized treatment and better outcomes for individuals with Crohn's disease.

Keywords: Crohn's disease, gut microbial dysbiosis, metabolomic signatures, magnetic resonance enterography, machine learning modelling

Graphical Abstract

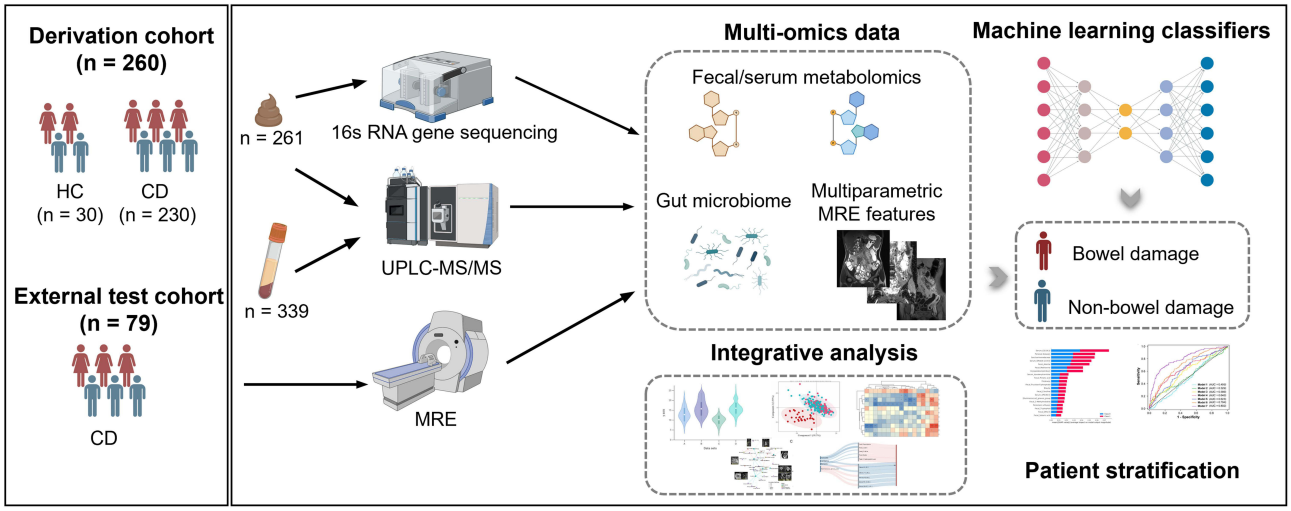

Introduction

Crohn's disease (CD) is a chronic and progressively debilitating inflammatory bowel disorder.[1] The global burden of CD is increasing, with rising prevalence observed not only in Europe and North America but also in newly industrialized countries.[1] Recurrent transmural inflammation is a key determinant in cumulative structural bowel damage (BD), giving rise to complications such as fibrotic strictures, abscesses, or fistulae.[2] Although advances in biologic therapies have improved disease control, many patients still progress to bowel damage over time,[3] which impairs intestinal function and eventually leads to long-term disability.[4] Therefore, precisely monitoring BD progression is crucial for optimizing CD management. Currently, the Lémann Index (LI) is the most widely recognized tool for assessing BD.[5–7] Despite its effectiveness, the calculation of LI relies heavily on extensive clinical data collected during a patient's prolonged illness. Obtaining accurate data becomes challenging when patients seek treatment across multiple healthcare facilities. This limitation underscores the need for an alternative approach that deepens our understanding of BD, and enables more effective monitoring and clinical management.

Magnetic resonance enterography (MRE) is an excellent non-invasive technique for repeated assessment of CD patients.[8] Multiparametric MRE captures macroscopic features, such as bowel wall thickening, perienteric edema, and complications, including fistulas and abscesses, which reflect structural damage and active inflammation.[9,10] Thus, MRE presents a critical tool for monitoring BD. However, a more precise assessment of BD can be achieved by integration of both macroscopic and microscopic data. While MRE provides valuable insights into macroscopic morphological

changes, it lacks the ability to provide detailed information on microscopic elements, such as multi-omics molecules. Additionally, it is crucial to ensure that the selected MRE features are directly linked to BD pathogenesis and are not merely coincidental.

The pivotal role of gut microbiome disturbances has been underscored in the onset and progression of CD.[11] CD-associated dysbiosis has been characterized by reduced gut bacterial diversity, together with loss of beneficial gut microbial genera and blooms of potential pathobionts. These microbial shifts contribute to chronic inflammation and gut barrier dysfunction, which can be exacerbated by metabolic alterations including dysregulation of bile acids, amino acids, sphingolipids, polyamines, and short-chain fatty acids (SCFAs).[11,12] The combined utility of microbial and metabolic biomarkers can distinguish CD from ulcerative colitis[13,14] or predict the efficacy of biologic therapies.[15] These results suggest that microbial and metabolic factors may be crucial in predicting BD.

In this prospective two-center study, we characterized the intestinal microbiota and fecal or serum metabolic profiles of 309 CD patients with or without BD and 30 healthy participants. We first delineated the specific intestinal microbiota, fecal and serum metabolites, and MRE features associated with BD defined by high-LI, aiming to elucidate how alterations in gut microbiota and their metabolic footprints contribute to BD-related MRE manifestations. Subsequently, we integrated diverse datasets, including clinical covariates, microbiota, fecal/serum metabolites, and MRE features, to construct 49 models using seven machine learning algorithms to identify the optimal approach for distinguishing BD from non-BD patients. Our findings demonstrate that a comprehensive model combining macroscopic and microscopic information from blood, fecal, and MRE examinations offers superior predictive performance for BD diagnosis in CD patients. This comprehensive approach highlights a promising alternative for BD severity stratification, potentially reducing the reliance on extensive clinical data and shedding light on the mechanistic underpinnings of intestine injuries in CD.

Materials and Methods

Participants Enrollment

We recruited two independent CD cohorts from the Yuexiu and Nansha campuses of the First Affiliated Hospital of Sun Yat-sen University between May 2021 and April 2023, serving as the derivation cohort for model development and test cohort for validation, respectively. The inclusion criteria were as follows: 1) adult CD patients (age >18 years); 2) ability to provide fecal or blood samples for analysis; and 3) underwent gastrointestinal endoscopy and MRE within one week of fecal/blood specimen collection. The exclusion criteria encompassed: 1) patients who had a medication history of antibiotics, probiotics, or prebiotics for over 3 days within 3 months before enrollment; or 2) those with concurrent organic or functional digestive diseases. Concurrently, healthy controls (HCs) with no abnormalities in physician inquiries, medication use and serum test indicators were recruited into the derivation cohort for comparison.

Clinical Data Acquisition

Demographic and clinical data of CD patients, including gender, age, body mass index (BMI), disease duration, surgical history, endoscopic findings, Montreal classification, Crohn's disease activity index (CDAI), erythrocyte sedimentation rate (ESR), and C-reactive protein (CRP) levels, were obtained from our hospital's information system. For HCs, data were obtained through physician interviews.

Lémann Index Scoring for BD Assessment

CD patients were divided into BD and non-BD (NBD) groups by LI, with a score >4.8 indicating BD and ≤4.8 indicating NBD.[7] LI, a standardized scoring system that quantifies the location, severity, and extent of cumulative BD using diagnostic imaging, endoscopy, and surgical history (Supplementary Table 1), was determined by a panel of experts, comprising three radiologists and one gastroenterologist with 5–10 years of IBD expertise.

MRE Protocols and Imaging Assessment for CD Patients

MRE was performed using a 3.0 T MRI device (MAGNETOM Prisma; Siemens Healthineers, Erlangen, Germany) equipped with an 18-channel abdominal coil. The scanning sequences included T2-weighted imaging (T2WI), diffusion-weighted imaging (DWI), and pre-/post-enhanced T1-weighted imaging (T1WI) (Supplementary Table 2).

To investigate the MRE features that can characterize BD, MRE characteristics of the most severe lesion, identified by the thickest bowel wall or narrowest bowel lumen, were evaluated to achieve consensus by three radiologists with 5–14 years of expertise. The recorded MRE features included bowel wall thickness, luminal stricture, penetrating lesions, perianal disease, bowel wall T2WI signal, perienteric effusion, arterial-phase enhancement pattern, lesion length, comb sign, and apparent diffusion coefficient (ADC) (detailed in Supplementary Table 3).

Fecal and Serum Samples Collection

A total of 261 fecal samples (derivation cohort, n=182; test cohort, n=79) and 339 serum samples (derivation cohort, n=260; test cohort, n=79) were collected. The participants provided blood or fecal specimens in the early morning, following an overnight fast. Fecal samples were immediately stored at −80 °C until further DNA extraction. Blood samples were clotted at room temperature for 30 min prior to centrifugation at 3500 rpm for 5 minutes to collect serum, which was stored at −80°C until metabolomic analysis.

Microbiome Analysis

All the samples were sequenced or measured in one batch, and processed using an identical bioinformatic pipeline. Fecal specimens were processed for total DNA extraction using the OMEGA Soil DNA Kit (Omega Bio-Tek, USA), following the manufacturer's protocol with minor modifications. DNA concentration and purity were measured using a NanoDrop 2000 spectrophotometer (Thermo Fisher Scientific) and the DNA integrity was confirmed by 1.2% agarose gel electrophoresis. The V3-V4 hypervariable regions of the 16S rRNA gene were amplified using the primers 338F (5'-ACTCCTACGGGAGGCAGCA-3') and 806R (5'-GGACTACHVGGGTWTCTAAT-3') by polymerase chain reaction (PCR).

The amplified products were purified using a magnetic bead-based purification system (Vazyme, China), and quantified using the Quant-iT PicoGreen dsDNA Assay Kit (Invitrogen). Sequencing libraries were constructed using the TruSeq Nano DNA LT Library Prep Kit (Illumina, San Diego, CA, USA) and sequenced on the Illumina NovaSeq 6000 platform using paired-end 2×250 bp sequencing. Raw sequence data were processed using QIIME2 and denoised with the DADA2 plugin, followed by taxonomic assignment using the SILVA 132 database. For taxonomic profiling, both amplicon sequence variant (ASV) and operational taxonomic unit (OTU) tables were used. Alpha diversity was described using Chao1, Simpson, and Pielou's evenness, and beta diversity was assessed using the Bray-Curtis distance matrix. Genera with an average relative abundance below 0.1% and prevalence of less than 10% were removed from the OTU table OTU data were log-ratio transformed before downstream analysis. Linear Discriminant Analysis (LDA) effect size (LEfSe) approach (LDA>2, $P<0.05$) and Mann–Whitney U-test with false discovery rate (FDR) correction (FDR<0.1) were used to discern the differentially abundant microbial taxa. Full experimental protocols for 16S rRNA gene sequencing and data analysis are available in Supplementary Method 1.

Metabolomic Profiling of Fecal and Serum Samples

Metabolomic profiling of fecal and serum samples was performed using targeted metabolomics with ultra-performance liquid chromatography coupled with tandem mass spectrometry (UPLC-MS/MS) system. A total of 233 fecal metabolites and 528 serum metabolites were detected. Orthogonal partial least squares discriminant analysis (OPLS-DA) and Mann–Whitney U-test were used to compare metabolite levels among groups. Important differential metabolites were screened based on variable importance (VIP) with a projection value of >1, a value of $P<0.05$, and FDR<0.2. Detailed metabolomic analysis protocols are provided in Supplementary Method 2.

Using Recursive Feature Elimination for BD Biomarker Identification

A matched panel of 152 CD patients with complete clinical, fecal, serum, and MRE data was assembled from the derivation cohort to identify biomarkers and construct a model for distinguishing BD from NBD. Feature selection was performed independently within each data type (clinical variables, microbiota, fecal metabolites, serum metabolites, and MRE features) using Recursive Feature Elimination (RFE) based on a Random Forest classifier (RFC) implemented in the scikit-learn package (v1.0.2) in Python (v3.7.9). For each data category, stratified 10-fold cross-validation (train: test = 9:1) was used during RFE to optimize feature selection. A total of 100 iterations with random seeds were conducted to ensure the robustness of the selection process, and features consistently ranked as important across all iterations were retained. The resulting feature sets from each biological source were subsequently used for constructing and comparing different multimodal integration models to predict BD status.

Development and Validation of Multi-Omics Model for BD Diagnosis

Using the refined feature set along with baseline clinical variables (age, gender, BMI, and lesion location), we developed seven types of predictive feature combinations to evaluate the incremental value of multidimensional data integration. These clinical covariates, although not all significantly different between BD and non-BD groups in our cohort, were retained in Model 1 to account for potential confounding and to ensure biological relevance and modeling stability.[16]

The models were constructed as follows:

Model 1: Clinical Covariates only.
Model 2: Clinical Covariates + Microbiota.
Model 3: Clinical Covariates + Fecal Metabolites.
Model 4: Clinical Covariates + Serum Metabolites.
Model 5: Clinical Covariates + MRE Features.
Model 6: Clinical Covariates + Microbiota + Fecal Metabolites + Serum Metabolites.
Model 7: Comprehensive Model including Clinical Covariates + Microbiota + Fecal Metabolites + Serum Metabolites + MRE Features.

Each model was trained and evaluated using seven machine-learning algorithms: RFC, Xtreme Gradient Boosting Classifier (XGBC), Decision Tree (DT), Radial Basis Function Support Vector Machine (RBF-SVM), Logistic Regression (LR), Linear-SVM, and K-nearest neighbors (KNN). To ensure model robustness and mitigate overfitting, we applied a nested 5-fold cross-validation strategy, where the inner loop optimized the model hyperparameters and the outer loop assessed the performance metrics. Performance metrics, including AUC, accuracy, sensitivity, specificity, positive predictive value, negative predictive value, and F1-score, were calculated. For the final model selection, the best-performing model, identified from the cross-validation folds, was applied to an independent external test cohort to assess its generalizability. Additionally, SHapley Additive exPlanations (SHAP) analysis was performed on the optimal model to interpret the feature contributions, and AUC comparisons across the models were assessed using DeLong's test.

Statistical Analysis

Statistical significance was determined using a two-tailed Mann–Whitney *U*-test for pairwise comparisons, the Kruskal–Wallis test for multigroup assessments, and Fisher's exact test for categorical data analysis. Spearman's partial correlation analysis was conducted to assess relationships among multi-omics data, adjusting for potential covariates, such as gender, age, BMI, smoking, and drinking history. Mediation analysis was conducted to assess the influence of bacterial genera on MRE features related to BD, with bacterial genera as the exposure, metabolites as mediators, and MRE features as the outcome (detailed in Supplementary Method 3). Statistical significance was set at $P<0.05$. Statistical analyses were performed using R version 4.3.1 or Python version 3.7.9.

Results

Patients Characteristics

Clinical and demographic data from the derivation and test cohorts are summarized in Table 1. A total of 339 participants were recruited in this study, comprising 230 CD patients and 30 age- and gender-matched HCs in the derivation cohort and

Table 1 Clinical Characteristics of All Participants in the Derivation and External Test Cohorts

Characteristics	Derivation Cohort (n = 260)				External Test Cohort (n = 79)		
	HCs (n = 30)	NBD (n = 127)	BD (n = 103)	*P*-value[b]	NBD (n = 46)	BD (n = 33)	*P*-value[c]
Gender, n (%)				0.97			0.84
Male	25 (83.3)	101 (79.5)	83 (80.6)		37 (80.4)	28 (84.9)	
Female	5 (16.7)	26 (20.5)	20 (19.4)		9 (19.6)	5 (15.1)	
Age (mean ± SD)	29 [24, 32]	30.3 ± 8.1	30.3 ± 7.9	0.97	28.9 ± 6.9	28.9 ± 6.7	0.99
BMI, kg/m^2 (median [IQR])	23.1 [21.3, 24.3]	19.9 [18.4, 21.9]	18.7 [17.2, 21.0]	0.05	19.2 [17.3, 21.6]	19.7 [18.4, 20.9]	0.37
Smoking history, n (%)	4 (13.3)	16 (12.6)	5 (4.9)	0.07	3 (6.5)	3 (9.1)	0.69
Drinking history, n (%)	5 (16.7)	11 (8.7)	5 (4.9)	0.39	1 (2.2)	1 (3.0)	1.00
Montreal classification, n (%)							
Age at diagnosis, n (%)	–			0.77			0.14
A1 [≤16]	–	3 (2.4)	1 (1.0)		0 (0)	0 (0)	
A2 [17–40]	–	110 (86.6)	92 (89.3)		42 (91.3)	33 (100)	
A3 [≥40]	–	14 (11.0)	10 (9.7)		4 (8.7)	0 (0)	
Location, n (%)	–			**0.01**			0.2
L1 [terminal ileum]	–	22 (17.3)	4 (3.9)		11 (23.9)	4 (12.1)	
L2 [colon]	–	4 (3.2)	5 (4.9)		2 (4.4)	4 (12.1)	
L3 [ileocolon]	–	96 (75.6)	90 (87.4)		33 (71.7)	24 (72.7)	
L4 [upper gastrointestinal]	–	5 (3.9)	4 (3.9)		0 (0)	1 (3.0)	
Behavior, n (%)				0.08			**0.01**
B1 [inflammatory]	–	56 (44.1)	33 (32.0)		23 (50.0)	10 (30.3)	
B2 [stricturing]	–	39 (30.7)	31 (30.1)		18 (39.1)	10 (30.3)	
B3 [penetrating]	–	32 (25.2)	39 (37.9)		5 (10.9)	13 (39.4)	
CDAI, n (%)				**0.001**			0.86
Remission [<150]	–	62 (50.4)	28 (27.5)		18 (39.1)	12 (36.4)	
Mild disease [150–220]	–	29 (23.6)	25 (24.5)		9 (19.6)	5 (15.2)	
Moderate disease [220–450]	–	32 (26.0)	48 (47.0)		18 (39.1)	16 (48.5)	
Severe disease [>450]	–	0 (0.0)	1 (1.0)		1 (2.2)	0 (0)	
Disease course, months (median [IQR])	–	40 [12, 96]	60 [24, 96]	0.23	41 [12, 72]	72 [24, 105]	0.16
Perianal disease, n (%)				**<0.001**			**<0.001**
None	–	74 (58.3)	13 (12.6)		32 (69.6)	9 (27.3)	
Anal fistula	–	45 (35.4)	70 (68.0)		12 (26.1)	20 (60.6)	
Perianal abscess	–	8 (6.3)	20 (19.4)		2 (4.4)	4 (12.1)	
Surgery, n (%)				**0.002**			**<0.001**
Intestinal surgery	–	26 (20.5)	33 (32.0)		4 (8.7)	13 (39.4)	
Perianal surgery	–	1 (0.9)	34 (33.0)		0 (0)	10 (30.3)	
Medication history [a], n (%)							
Biologics	–	34 (33.3)	29 (41.4)	0.93	19 (41.3)	16 (48.5)	0.69
Corticosteroids	–	5 (6.3)	7 (14.0)	0.50	2 (4.4)	1 (3.0)	1.00
Immunomodulator	–	44 (51.8)	25 (59.5)	0.12	8 (17.4)	6 (18.2)	1.00
5-Aminosalicylic Acid	–	20 (30.8)	16 (51.6)	0.96	12 (26.1)	8 (24.2)	1.00
Laboratory index							
CRP, mg/L (median [IQR])	–	2.9 [0.7, 14.7]	13.83 [3.7, 34.2]	**<0.001**	2.8 [0.9, 12]	3.14 [1.1, 21.2]	0.30
ESR, mm/h (median [IQR])	–	14 [6, 31]	32 [16, 58]	**<0.001**	11 [4.3, 24.5]	15 [4, 32]	0.34
Hb, g/L (median [IQR])	–	131 [117, 141]	120 [99, 134]	**0.001**	131.5 [116.3, 144.5]	128 [107, 140]	0.33
ALB, g/L (median [IQR])	–	38.8 [35.9, 40.8]	35.9 [32.1, 39.7]	**0.003**	38.8 [35.9, 41.6]	39.5 [33.9, 41.7]	0.56

Notes: [a]Medicine use within three months prior to inclusion. [b]*P*-values calculated for the comparison between BD and NBD groups within the derivation cohort. [c]*P*-values represent comparison between BD and NBD groups in the external test cohort. Continuous variables were analyzed using the *t*-test or Mann–Whitney *U*-test, and categorical variables were analyzed using the chi-squared test or Fisher's exact test, as appropriate. Bolded P values indicate statistically significant differences ($P<0.05$).
Abbreviations: HCs, healthy controls; BD, bowel damage; NBD, non-bowel damage; CD, Crohn's disease; IQR, interquartile range; BMI, body mass index; CDAI, Crohn's disease activity index; CRP, C-reactive protein; ESR, erythrocyte sedimentation rate; Hb, hemoglobin; ALB, albumin.

79 CD patients in the test cohort. Based on the LI evaluation, 103 patients in the derivation cohort were classified as BD group and 127 as NBD group, whereas the test cohort included 33 BD and 46 NBD patients (Figure 1).

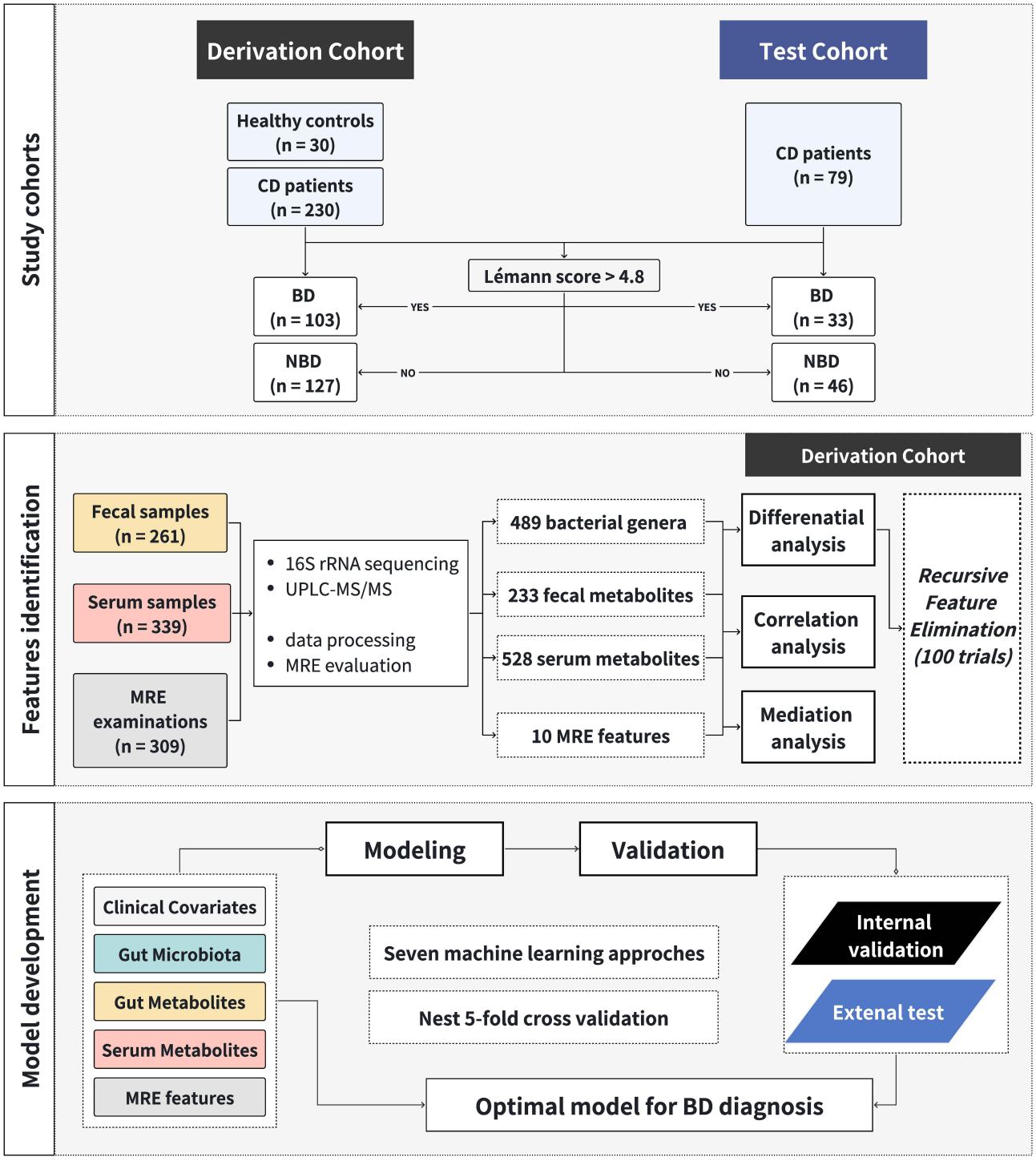

Figure 1 Flowchart depicting participants recruitment and study design.

Differentiation of MRE Characteristics Between BD and NBD Patients

In the MRE features for CD patients, seven exhibited significant differences between the NBD and BD groups, including perianal diseases, perienteric effusion, bowel wall thickness, comb sign, bowel length, bowel wall T2WI signal, and penetration (all $P<0.05$; Table 2). Overall, patients with BD exhibited a more aggressive imaging phenotype with distinct MRE manifestations than those with NBD. BD patients were characterized by greater bowel wall thickening, longer segments of bowel involvement, and a higher mural T2WI signal, indicating more severe intestinal inflammation. The

https://doi.org/10.2147/JIR.S524671

Table 2 Differentiation of MRE Characteristics Between BD and NBD Patients in Derivation Cohort

MRE features	NBD (n=127)	BD (n=103)	*P*-value
Stricture, n (%)			0.224
None	58 (45.7)	36 (35.0)	
Without pre-stenotic dilation	27 (21.2)	29 (28.1)	
With pre-stenotic dilation	42 (33.1)	38 (36.9)	
Penetration, n (%)			**0.046**
None	16 (12.6)	8 (7.8)	
Deep ulcer	89 (70.1)	67 (65.0)	
Fistula or abscess	22 (17.3)	28 (27.2)	
Bowel wall T2WI signal, n (%)			**0.043**
Similar to the normal bowel	44 (34.6)	23 (22.3)	
Higher than the normal bowel	83 (65.4)	80 (77.7)	
Perienteric effusion, n (%)			**0.003**
Similar to the normal mesentery	85 (66.9)	46 (44.7)	
Increased mesenteric signal without perienteric effusion	23 (18.1)	31 (30.1)	
Increased mesenteric signal with perienteric effusion	19 (15.0)	26 (25.2)	
Bowel wall enhanced pattern, n (%)			0.074
Homogeneous enhancement	94 (74.0)	66 (64.1)	
Mucosal enhancement	17 (13.4)	26 (25.2)	
Layered enhancement	16 (12.6)	11 (10.7)	
Bowel Length, n (%)			**0.042**
≤15 cm	104 (81.9)	72 (69.9)	
>15cm	23 (18.1)	31 (30.1)	
Comb sign, n (%)			**0.033**
None	78 (61.4)	48 (46.6)	
Yes	49 (38.6)	55 (53.4)	
ADC (median [IQR])	1.09 [0.95, 1.30]	1.08 [0.98, 1.24]	0.610
Thickness (median [IQR])	6.00 [4.00, 7.60]	7.00 [5.25, 8.30]	**0.010**
Perianal diseases, n (%)			**<0.001**
None	69 (54.3)	16 (15.5)	
Fistula	49 (38.6)	67 (65.1)	
Abscess	9 (7.1)	20 (19.4)	

Notes: The Fisher' s test and Kruskal–Wallis non-parametric test were used for analysis of qualitative and quantitative data, respectively. Statistically significant values ($P<0.05$) are highlighted in bold.

Abbreviations: CD, Crohn' s disease; MRE, magnetic resonance enterography; NBD, non-bowel damage; BD, bowel damage; T2WI, T2-weighted imaging; ADC, apparent diffusion coefficient; IQR, interquartile range.

presence of perienteric effusion and comb sign reflected increased mesenteric involvement and vascularity, both of which are markers of active disease. Penetrating complications, including fistulas and abscesses, were more frequently observed in BD patients, along with a markedly higher incidence of perianal disease. These results further underscore the strong association between the MRE features and the presence of BD.

Distinct Microbiome Alterations Between NBD and BD Patients

To investigate microbiome trait alterations from HCs to patients with NBD and then to patients with BD, α- and β-diversity were assessed. We observed reduced α-diversity in the gut microbiota of CD patients compared to that in HCs, as indicated by lower Chao1, Simpson, and Pielou's evenness indices (all $P<0.001$; Figure 2A). Notably, significant reductions in Pielou's evenness and Simpson index were also found in BD patients compared to those in NBD patients (both $P<0.05$). β-Diversity analysis revealed distinct bacterial community compositions among the three groups (all $P<0.05$; Figure 2B). Furthermore, we observed variations in the gut microbial profiles from phylum to genus levels among the three groups (Figure 2C), providing visual evidence of microbial shifts associated with BD. These trends,

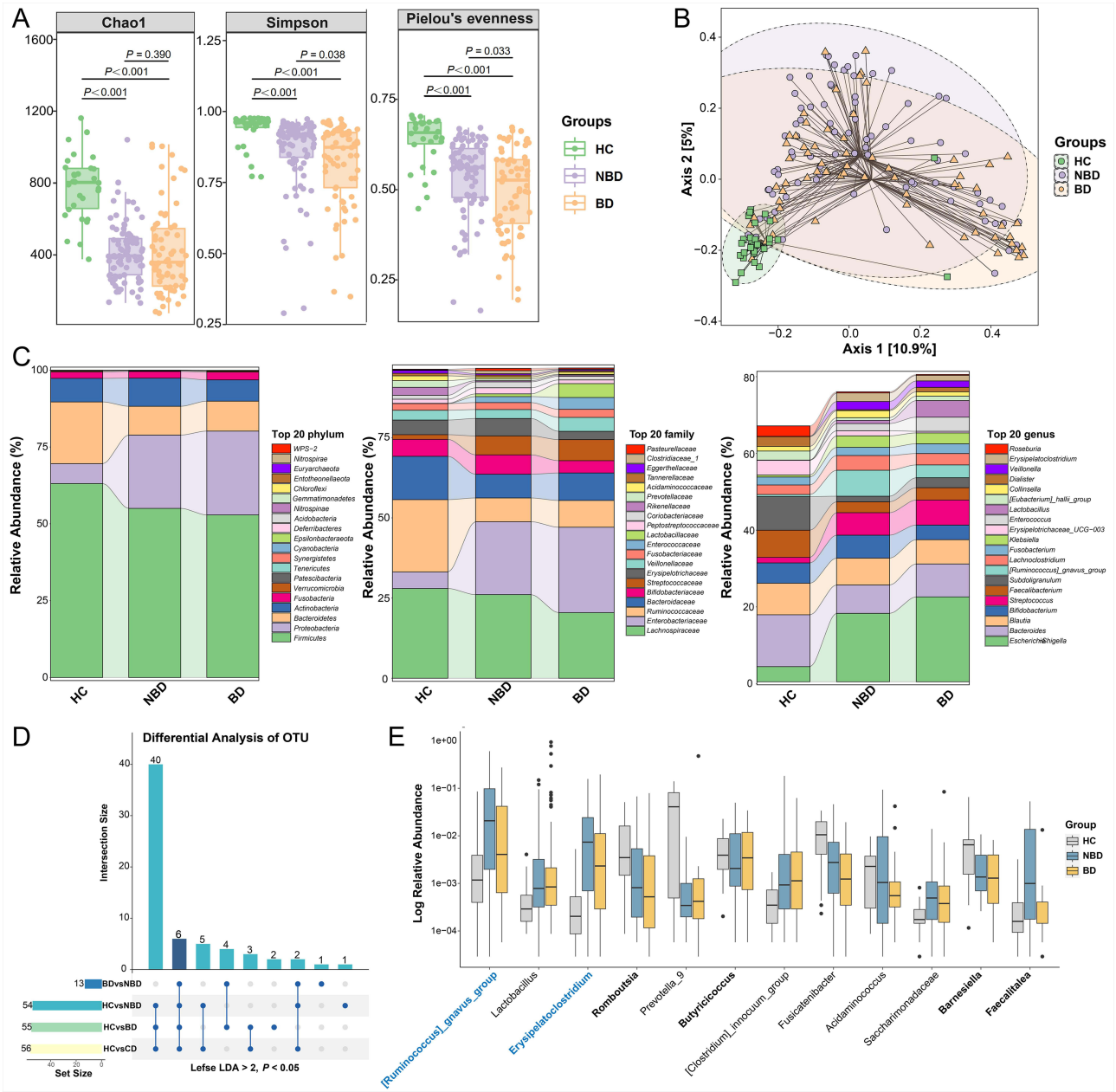

Figure 2 Differential gut microbiota traits in CD patients with or without BD compared to HCs. (**A**) Box plots of alpha diversity indices (Chao1, Simpson, and Pielou's evenness) demonstrate reduced richness, significantly decreased diversity, and evenness in the BD group compared to the NBD and HCs groups. (**B**) Principal Coordinates Analysis (PCoA) plot based on Bray-Curtis Distance Matrix reveals differences in beta diversity of gut microbiota between HCs and both NBD and BD (both *P*=0.001), and between NBD and BD (*P*=0.038). Percentages in parentheses in axis labels show the proportion of explained dis-similarity data (10.9% and 5%). Closer points indicate greater similarity, while dashed ellipses represent 95% confidence intervals. (**C**) Bar charts showing the distribution of the top 20 phylum, family, and genus across the three groups. The y-axis represents the percentage of relative abun-dance attributed to different phylum, family, and genus. Distinct taxonomic units are color-coded. (**D**) The differential analysis identified six microbial genera using Linear Discriminant Analysis (LDA) effect size (LEfSe) analysis (LDA score>2, *P*<0.05), depicted in the upset plot. Vertical bars represent the number of intersecting operational taxonomic units (OTUs) across differential analyses among the groups: HCs vs CD, HCs vs BD, HCs vs NBD, and BD vs NBD, as indicated by the connected circles below the histogram. Dark blue bars denote OTUs that overlap among all four comparisons, while horizontal bars display the OTU set size. (**E**) Bar charts showing the log relative abundances of 12 discriminatory microbial genera associated with BD by using LEfSe analysis (6 genus depicted in bold) and Mann–Whitney *U*-test across the group comparisons (FDR<0.1, 8 genus). The intersecting genus of the two approaches are depicted in blue.

including increased *Proteobacteria* and *Fusobacteria* and decreased *Firmicutes* and *Bacteroidetes*, aligned with the known microbial dysbiosis in inflammatory bowel diseases.[17]

To identify more reliable microbial markers, we employed LEfSe analysis to reveal significant differences in the relative abundances of six key bacterial genera across various group comparisons (HCs vs CD, HCs vs BD, HCs vs

https://doi.org/10.2147/JIR.S524671

NBD, and BD vs NBD; Figure 2D, Supplementary Figure 1). Additionally, the Mann–Whitney *U*-test was applied to refine these results and highlight eight genera with significant differences between groups ($P<0.05$, FDR<0.1; Supplementary Figure 2). The intersection of these analyses identified *[Ruminococcus]_gnavus_group* (*R. gnavus*) and *Erysipelatoclostridium* as potential microbial biomarkers for characterizing BD. These two genera, along with *Saccharimonadaceae* and *Faecalitalea*, exhibited the lowest abundances in HCs, significantly increased in NBD, and then decreased in BD, but remained higher than that in HCs. Other genera, such as *Romboutsia* and *Prevotella_9*, were lower in the CD group than in the HC group and showed further reduction in the BD group compared to the NBD group (all $P<0.05$; Figure 2E). These findings delineate specific microbial signatures in patients with BD, highlighting their vital role in BD diagnosis.

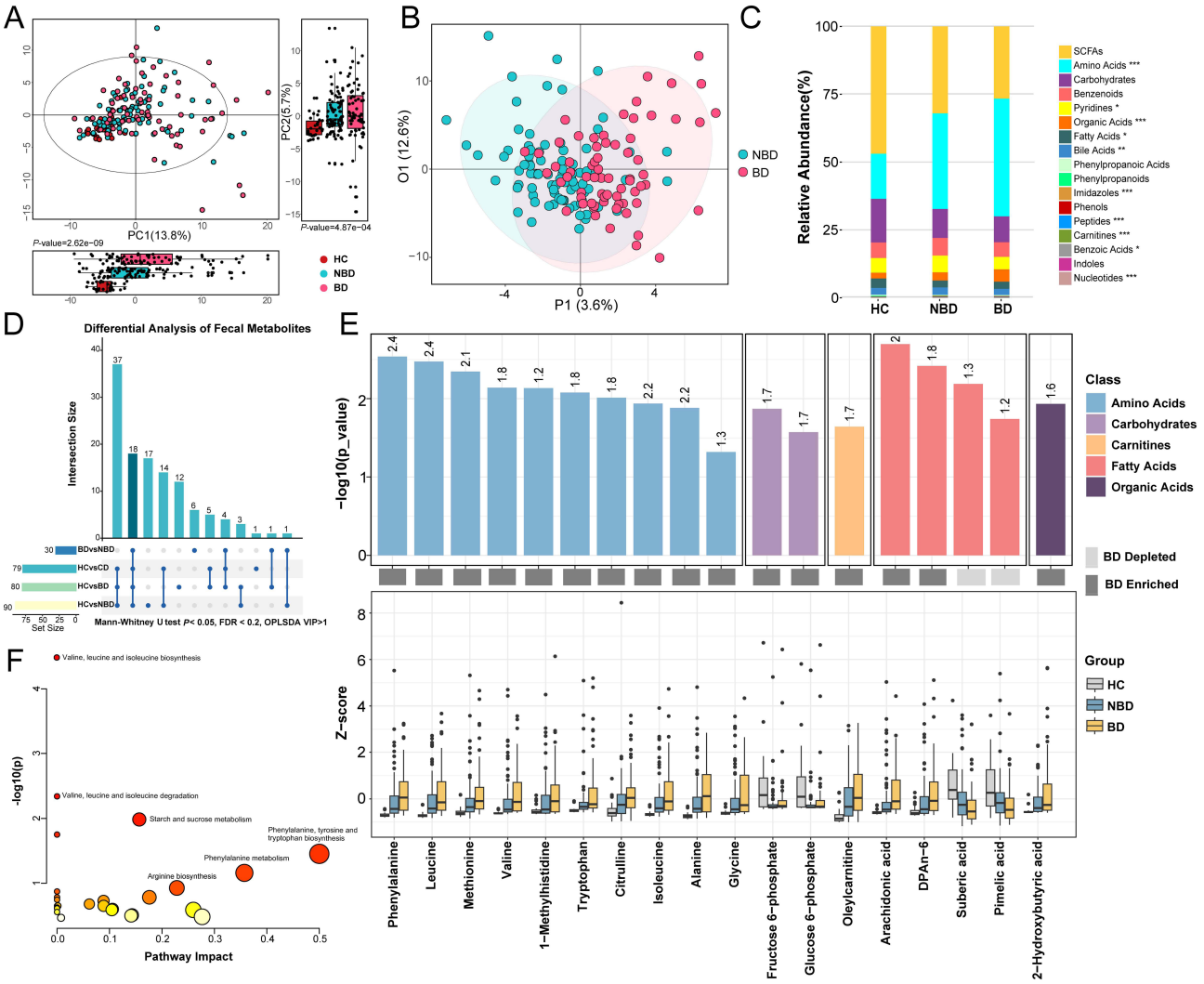

Figure 3 Fecal metabolomic profiles and pathway enrichment analysis between NBD and BD patients. (**A**) Principal component analysis (PCA) Score Plot displaying the separation among HCs, NBD, and BD groups. PC1 (x-axis) accounts for 13.8% of the variance, and PC2 (y-axis) explains 5.7%. Box plots on the right and bottom depict the distribution of scores along PC2 and PC1. *P* values (4.87e-04 for PC2, 2.62e-09 for PC1) indicate significant differences among the groups. (**B**) Orthogonal Partial Least Squares Discriminant Analysis (OPLS-DA) Score Plot illustrating the metabolic profile separation between NBD and BD. (**C**) Stacked Bar Chart showing the relative abundance (%) of fecal metabolite classes among HCs, NBD, and BD. Variations in amino acids, organic acids, imidazoles, peptides, carnitines, benzoic acids, and nucleotides are marked (* FDR<0.05, ** FDR<0.01, *** FDR<0.001). (**D**) Upset Plot for differential analysis of fecal metabolites across groups: BD vs NBD, HCs vs CD, HCs vs BD, and HCs vs NBD. Bar chart shows shared metabolites (intersection size). Set size represents total significant metabolites per comparison. Significance determined by Mann–Whitney *U*-test ($P<0.05$, FDR<0.2), and an OPLS-DA model with a Variable Importance in Projection (VIP) score > 1. Connected dots represent shared metabolites. (**E**) Shared Differential Metabolites Analysis of 18 fecal metabolites across group comparisons. Top panel shows -log10(P-value) for each metabolite. Numbers above bars represent VIP scores from OPLS-DA. Bars labeled "BD Depleted" or "BD Enriched" indicate metabolite changes in BD compared to NBD. Bottom panel displays Z-scores for each metabolite. (**F**) Pathway Enrichment Analysis using the 18 significantly altered metabo-lites between BD and NBD.

Altered Fecal Metabolomic Profile Reveals Amino Acid Dysregulation Linked to BD in CD Patients

We then performed metabolomic analysis of fecal samples. In the fecal metabolome, 233 metabolites were detected and showed increasing trends from HCs to patients with NBD and then to patients with BD, indicating a systematic shift in fecal metabolic profiles with disease progression (Figure 3A). OPLS-DA further confirmed a distinction in the fecal metabolomic profiles between BD and NBD (Figure 3B). The relative abundance distribution of fecal metabolite classes among the three groups is displayed in Figure 3C. BD patients exhibited increased levels of amino acids, organic acids, and peptides compared to HCs and NBD patients (FDR<0.001). Next, we identified 79, 90, 80, and 30 differential fecal metabolites for HCs vs CD, HCs vs NBD, HCs vs BD, and BD vs NBD comparisons, respectively (VIP score>1, P<0.05; Figure 3D). Among these, 18 metabolites demonstrated consistent differential expression across comparisons, and were mainly classified as amino acids, fatty acids, carbohydrates, organic acids, and carnitines (Figure 3E). Sixteen metabolites were upregulated, while two (pimelic acid and suberic acid) were downregulated in BD compared with NBD. Fecal metabolomic pathway analysis based on differential metabolites revealed significant enrichment of pathways (Figure 3F), particularly "phenylalanine, tyrosine, and tryptophan biosynthesis" (Impact=0.500, P=0.035). These results indicate that BD is associated with significant alterations in fecal metabolites, particularly increased levels of aromatic amino acids, which may contribute to gut barrier disruption and heightened immune activation, potentially exacerbating local inflammation and disease severity.

Serum Metabolomics Identifies Crucial Lipid Metabolism Perturbations Underpinning BD in CD Patients

In total, 528 metabolites were identified in the serum metabolome. Similarly, the principal component analysis (PCA) plot revealed distinct separation between the three groups (Figure 4A). OPLS-DA further confirmed the distinction in the serum metabolomic profiles between BD and NBD (P<0.001; Figure 4B). Significant differences in amino acids, benzoic acids, carbohydrates, cholesteryl esters (CE), ceramides (Cer), indoles, and sphingomyelins (SM) were observed among the three groups (FDR<0.001; Figure 4C). We identified 165, 178, 179, and 122 differential metabolites in comparisons between HCs and CD, HCs and NBD, HCs and BD, and BD and NBD, respectively (VIP score>1, P<0.05; Figure 4D). A common intersection of 67 differential metabolites was identified (Figure 4D and E), predominantly from the SM, phosphatidylcholines (PC), phosphatidylethanolamines (PE), CE, Cer, and lysophosphatidylcholines (LPC) classes. Except for N-acetylneuraminic acid and pelargonic acid, the differential metabolites exhibited a declining trend across the HC, NBD, and BD groups. Metabolomics pathway analysis emphasized significant disruptions in "Glycerophospholipid metabolism" (Impact=0.216, P=0.001), "Ether lipid metabolism" (Impact=0.289, P=0.006), and "Sphingolipid metabolism" (Impact=0.216, P=0.016) pathway (Figure 4F), underscoring the critical roles of lipid metabolic processes in BD progression.

Microbiome-Metabolomics Interactions Highlight Key Pathways Contributing to BD Pathogenesis

To explore the interaction between gut bacteria and metabolites in patients with BD, Spearman's partial correlation analysis was employed by adjusting for potential confounders, including sex, age, BMI, smoking history, and drinking history. We observed significant positive correlations between bacterial genera *Erysipelatoclostridium, R. gnavus*, and *[Clostridium]_innocuum_group* (*C. innocuum*) with various altered serum metabolites, including SM, PE, PC, and phosphatidylserines (PS) (Figure 5A). Notably, these genera showed a strong correlation with ePE(38:1) (all r>0.34, P<0.01), suggesting their involvement in lipid metabolism regulation in BD. Interestingly, *C. innocuum* demonstrated a significant positive association with specific fecal suberic acid (r=0.518) and pimelic acid (r=0.515), which are intermediates of fatty acid metabolism,[18] and an inverse relationship with fecal arachidonic acid (r=−0.499) and DPAn-6 (r=−0.418), which are polyunsaturated fatty acids involved in inflammatory pathways and lipid signaling[19,20] (all P<0.001; Figure 5B). This dual association indicates that *C. innocuum* may influence lipid metabolic pathways through its interactions with systemic (serum) metabolites and within the local intestinal environment (fecal metabolites), which is consistent with previous studies.[20,21] Moreover, *Fusicatenibacter* was negatively correlated with several fecal

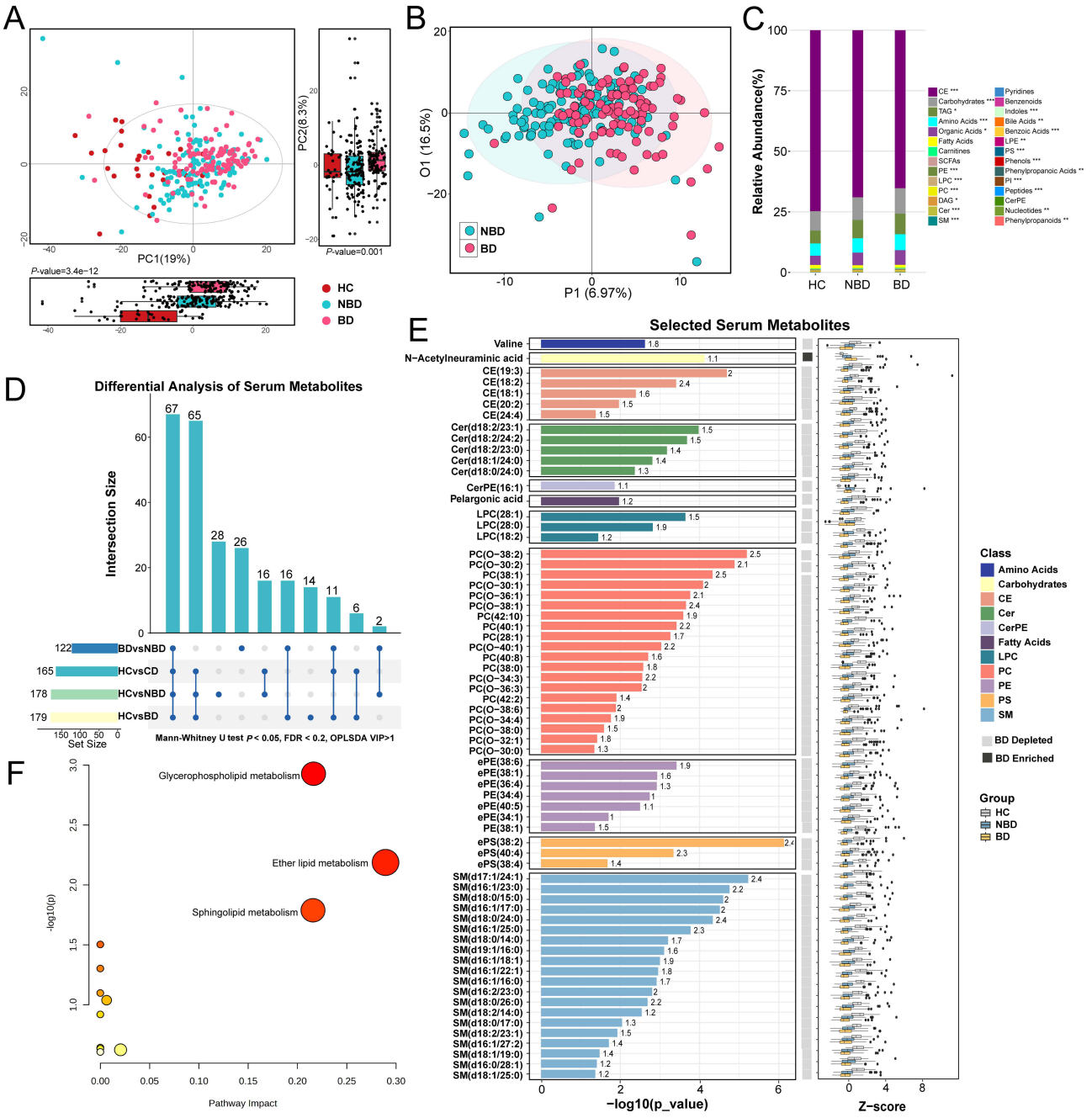

Figure 4 Serum metabolomic profiles and pathway enrichment analysis between NBD and BD patients. (**A**) PCA Score Plot displaying the separation among HCs, NBD, and BD groups. PC1 accounts for 19% of the variance, while PC2 explains 8.3%. Box plots on the right and bottom show PC2 and PC1 score distributions. Significant P-values (3.14e-12 for PC2 and 0.001 for PC1) indicate differences between groups. (**B**) OPLS-DA model illustrating the serum metabolic profile separation between NBD and BD. (**C**) Stacked Bar Chart depicting the relative abundance (%) of various serum metabolite classes among HCs, NBD, and BD groups. Significant variations in metabolite classes are depicted (* FDR<0.05, ** FDR<0.01, *** FDR<0.001). (**D**) Upset Plot for differential analysis of serum metabolites across different groups: BD vs NBD, HCs vs CD, HCs vs BD, and HCs vs NBD. The bar chart indicates the number of significant metabolites shared among comparisons (intersection size). The set size at the bottom represents the total number of significant metabolites in each comparison. Significance was determined using the Mann–Whitney *U*-test (P<0.05, FDR<0.2), and OPLS-DA model (VIP score>1). The connected dots represent shared metabolites between groups. (**E**) The 67 significant serum metabolites across group comparisons are exhibited. The top panel shows the -log10(P-value) for each metabolite, with numbers above bars representing the VIP scores from OPLS-DA analysis. Bars labeled "BD Depleted" or "BD Enriched" indicate whether the metabolite is decreased or increased in the BD group compared to the NBD group. The bottom panel displays Z-scores for each metabolite, showing the relative abundance and variation among the groups. (**F**) Pathway enrichment analysis using significantly 67 altered metabolites between BD and NBD. Significant pathways are indicated (P<0.05).

amino acids, such as glycine (r=−0.456, P<0.001), alanine (r=−0.383, P<0.01), phenylalanine (r=−0.360, P<0.01), and valine (r=−0.349, P<0.01), highlighting its role in influencing amino acid metabolism and potentially affecting BD.

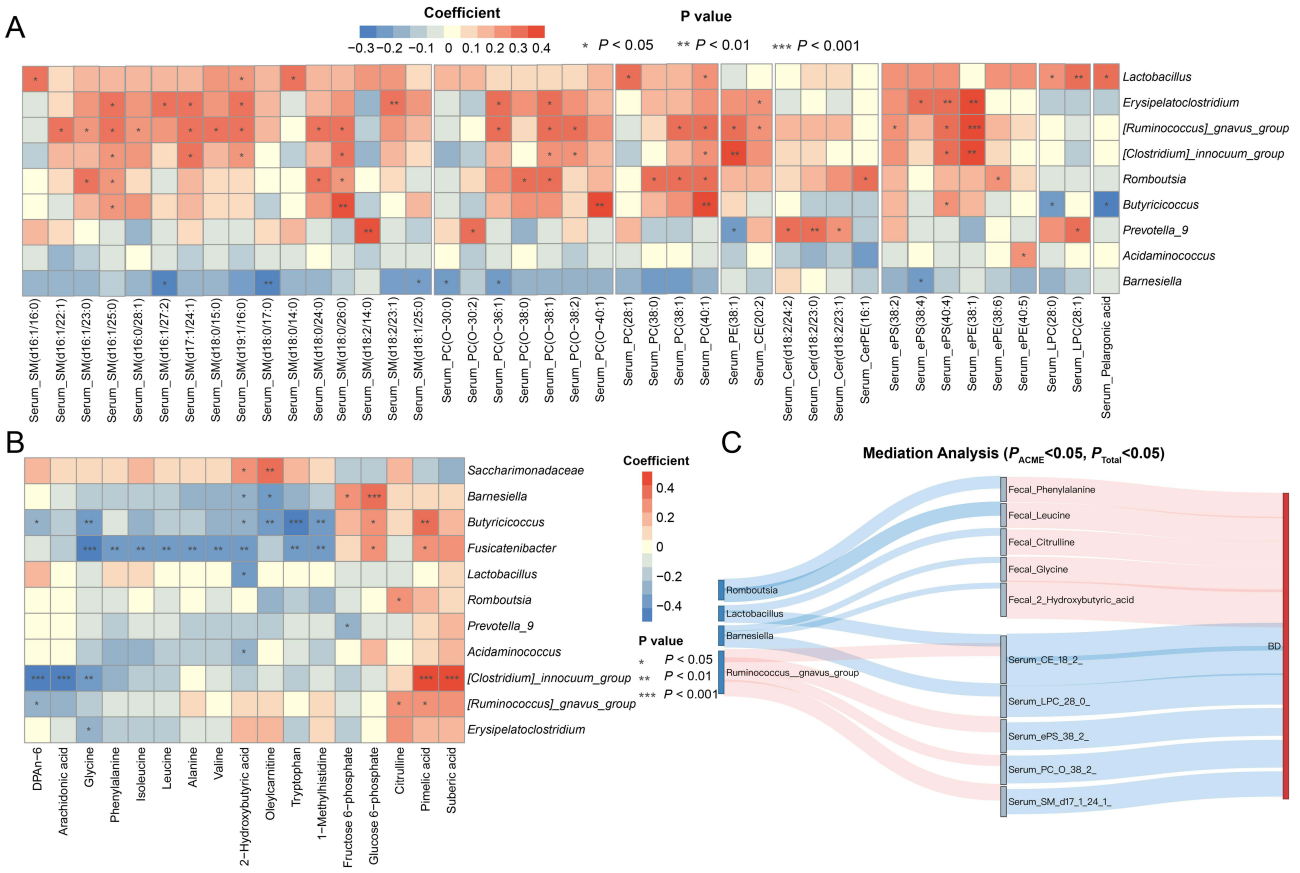

Figure 5 The interrelationship among the disturbed gut microbiota, fecal, serum metabolite in BD patients. (**A**) Heatmap of correlation analysis between serum metabolites and gut microbiota and (**B**) heatmap of correlation analysis between fecal metabolites and gut microbiota, both performed using Spearman partial correlation analysis with adjustments for confounders (gender, age, BMI, smoking, and drinking history). The color scale represents the correlation coefficient (blue for negative, red for positive). Significant correlations are denoted by * P<0.05, ** P<0.01, *** P<0.001. (**C**) Mediation Analysis showing the relationships between specific fecal metabolites, serum metabolites, and BD. The color scale represents the correlation coefficient (blue for negative, red for positive). Significant mediation effects are indicated (P_{ACME}<0.05, P_{Total}<0.05).

Mediation analysis revealed the role of specific bacterial genera in modulating metabolites and their effect on BD (Figure 5C, Supplementary Table 4). These results demonstrated that reduced *R. gnavus* may contribute to BD by decreasing the levels of several serum metabolites related to lipid metabolism. For instance, significant associations were observed between reduced levels of PC(O-38:2) (P_{ACME}=0.007, P_{Total}=0.010) and SM(d17:1/24:1) (P_{ACME}=0.010, P_{Total}=0.010), supporting the involvement of this genus in lipid metabolism disturbances in BD. These results characterized microbial-metabolite interactions in BD and provided evidence that the gut microbiota and metabolites can differentiate BD from NBD.

Microbiome-Metabolomics Biomarkers Linked to BD-Related Morphological Changes Observed on MRE

To determine the reliability of MRE features related to BD, we analyzed the links between microscopic traits and macroscopic MRE features. 29 multi-omics biomarkers were significantly associated with seven MRE features (0.25<|r|<1, all P<0.05), including 6 bacterial genera, 5 fecal metabolites, and 18 serum metabolites (Figure 6A). The interaction among these bacterial, metabolic biomarkers, and MRE features are intuitively displayed in a network graph (Figure 6B, Supplementary Table 5). Notably, the pro-inflammatory *Erysipelatoclostridium* was positively correlated with bowel wall thickness (r=0.380, P=0.002), T2WI signal (r=0.299, P=0.017), and perienteric effusion (r=0.331, P=0.008), which are important MRE indicators of intestinal inflammation. Similarly, *Barnesiella* was positively associated with the comb sign (r=0.38, P = 0.001), length (r=0.37, P=0.002), and bowel wall T2WI signal (r=0.40, P=0.001), suggesting that higher

https://doi.org/10.2147/JIR.S524671

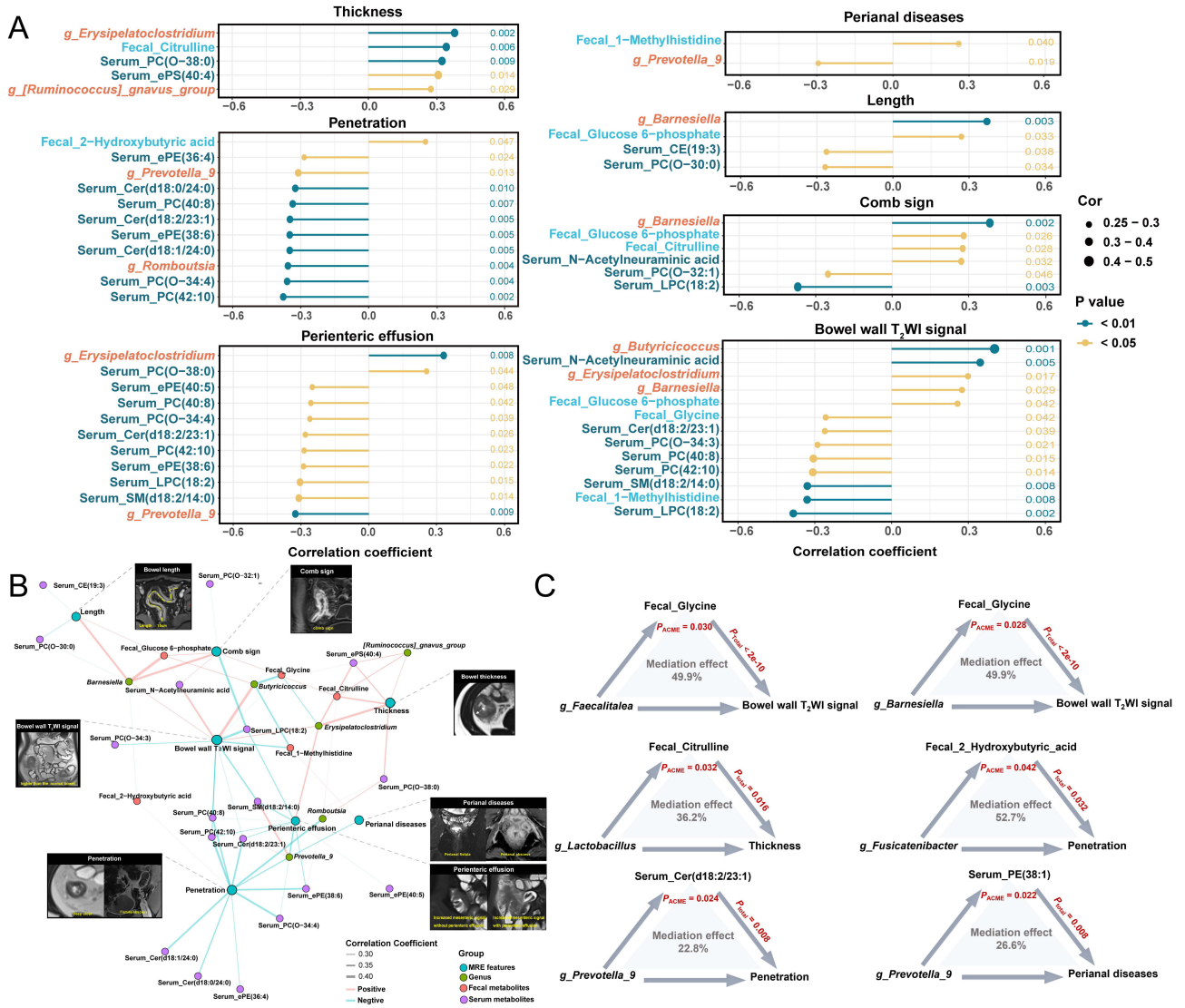

Figure 6 Correlation and mediation analysis of gut microbiota, metabolites, and MRE features in BD patients. (**A**) Lollipop diagram indicating correlation coefficients between MRE features (thickness, penetration, perianal diseases, length, comb sign, perienteric effusion, and bowel wall T2WI signal) and significant gut microbiota (red), fecal metabolites (light blue), and serum metabolites (blue). The size of the dots indicates the correlation coefficient strength. Significant correlations are marked with different colors of circles. (**B**) Network Visualization of significant correlations among serum metabolites, fecal metabolites, gut microbiota, and MRE features ($0.25<|r|<1$, $P<0.05$). Each node represents a variable, and edges represent significant correlations, with line thickness corresponding to the strength of the correlation. (**C**) Mediation analysis showing the mediation effects of specific metabolites on the relationship between clinical indicators and BD. Significant mediation effects are indicated ($P_{ACME}<0.05$, $P_{Total}<0.05$).

levels of *Barnesiella* contribute to inflammatory processes in the bowel vasculature and are linked to more extensive bowel involvement. In contrast, *Prevotella_9* was negatively correlated with perianal diseases and penetrating lesions, suggesting that higher levels of *Prevotella_9* were associated with a lower incidence of these complications. In addition, the observed negative correlations between multiple serum lipid metabolic markers, such as PC(40:8), PC(42:10), and ePE(38:6), and key MRE indicators, such as penetration, perienteric effusion, and bowel wall T2WI signal, underscore that reduced levels of these specific phospholipids are linked with more severe disease manifestations. Moreover, the negative correlations between serum ceramides, such as Cer(d18:1/24:0), and both T2WI signal and penetration suggest that ceramides may play a protective role in mitigating extreme inflammatory and structural damage.

Mediation analysis revealed how gut microbiota affected BD-related morphological changes through metabolites (Figure 6C, Supplementary Table 6). *Prevotella_9* was associated with penetration and perianal disease through serum ceramide (d18:2/23:1) (P_{ACME}=0.024, P_{Total}=0.008) and serum PE(38:1) (P_{ACME}=0.022, P_{Total}=0.008), with mediation

effects of 22.8% and 26.6%, respectively. Besides, *Fusicatenibacter* might influence penetration through fecal 2-hydroxybutyric acid (P_{ACME}=0.042, P_{Total}=0.032, mediation effect = 52.7%). These observations validated the pathophysiological basis of the selected MRE features linked to BD at the microbiota and metabolite levels, further confirming their reliability as predicting indicators of BD.

Linking Multi-Omics Model to MRE Features for Enhancing BD Prediction Efficacy

Capitalizing on the discriminative power of gut microbiota, metabolites, and MRE features between BD and NBD patients, we employed RFE-enhanced RFC to identify optimal biomarkers. The final panel comprised 3 microbial genera (*R. gnavus, Erysipelatoclostridium, Saccharimonadaceae*), 6 fecal metabolites (Alanine, Pimelic acid, suberic acid, arachidonic acid, glucose 6-phosphate, 1-Methylhistidine), 3 serum metabolites (CE(19:3), ePE(36:4), and ePS(38:2)), and 3 MRE features (ADC, thickness, and perianal diseases) (Supplementary Figure 3).

To identify the optimal modeling strategy, we constructed seven models (Model 1 to Model 7) based on progressively integrated clinical, microbiome, metabolomic, and imaging features. Across these models, we evaluated seven classification algorithms, resulting in 49 model-algorithm combinations trained on the derivation cohort. In internal validation, XGBC and RFC consistently outperformed the other classifiers, particularly in Model 7 (AUC: 0.857 vs 0.869), with high accuracy (0.796 vs 0.770) and F1-scores (0.774 vs 0.737) (Supplementary Table 7). We then benchmarked XGBC and RFC across all seven models in the external test cohort. XGBC outperformed RFC across all models, with the greatest advantage observed in Model 7 (AUC: 0.829 vs 0.815; accuracy: 0.759 vs 0.747; F1-score: 0.655 vs 0.630) (Supplementary Table 8). Based on its consistent performance across datasets, XGBC was selected as the optimal classification algorithm.

Subsequently, we used XGBC to visualize and compare the performance of Model 1-Model 7. As shown in Figure 7A and B, ROC curve analyses revealed stepwise improvements in AUC with increasing data integration, with Model 7 achieving the highest performance compared to the other six models (AUCs in the derivation cohort: 0.516–0.777; AUCs in the external test

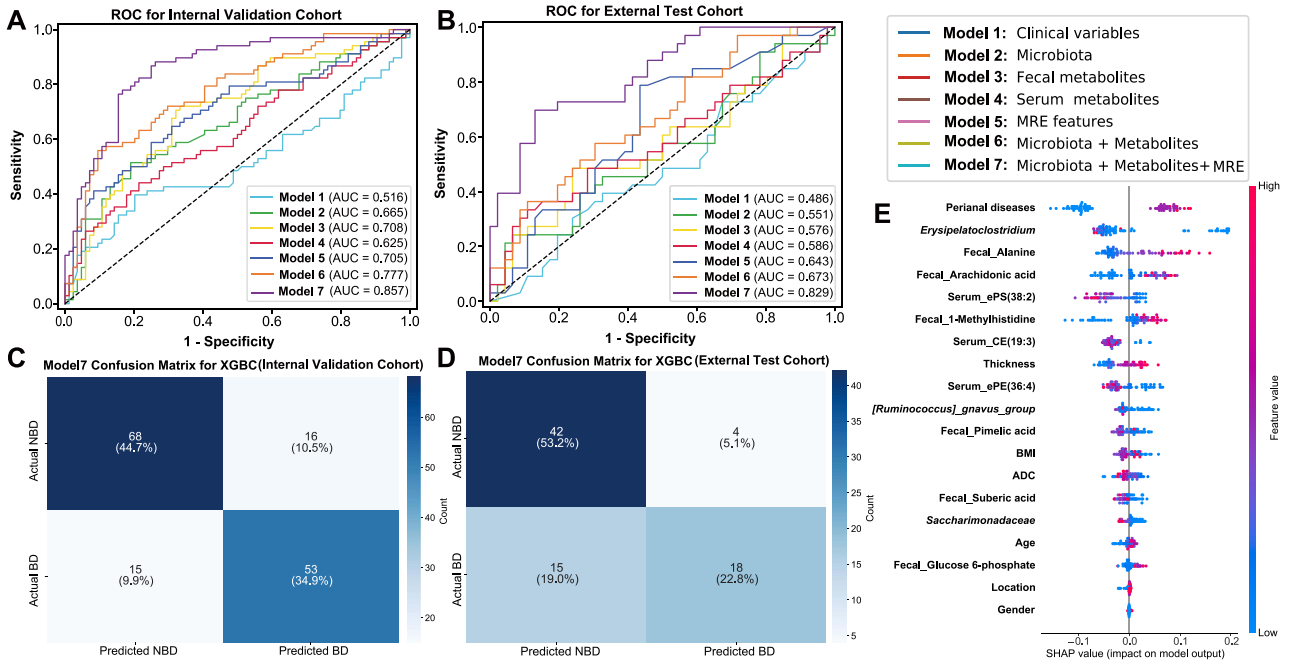

Figure 7 Performance and interpretability of optimal model distinguishing BD from NBD in CD patients. (**A**) and (**B**) present the receiver operating characteristic (ROC) curves for Models 1–7 in the internal validation cohort (**A**) and the external test cohort (**B**), with the area under the curve (AUC) values indicated for each model. Model 1 uses clinical covariates only, Model 2 incorporates microbiota, Model 3 integrates fecal metabolites, Model 4 includes serum metabolites, Model 5 combines magnetic resonance enterography (MRE) features, Model 6 merges microbiota and metabolites, and Model 7 is the comprehensive model, combining microbiota, metabolites, and MRE features. (**C**) and (**D**) present the confusion matrices for Model 7 in the internal validation cohort (**C**) and external test cohort (**D**), respectively. The matrices show the number and percentage of correctly and incorrectly predicted classes, with color intensity proportional to the case count. (**E**) SHapley Additive exPlanations (SHAP) plot for the XGBC-based Model 7, illustrating the contributions of individual features to the predictive output. Red dots represent higher values of the feature, while blue dots represent lower values. Features with higher SHAP values exert greater influence on model decision-making.

https://doi.org/10.2147/JIR.S524671

cohort: 0.486–0.673). Confusion matrices for XGBC-based Model 7 (Figure 7C and D) further confirmed its clinical utility for BD prediction, with a PPV of 81.8% and NPV of 73.7% in the test cohort. For comparison, confusion matrices for XGBC-based Models 1–6 are provided in Supplementary Figures 4 and 5.

SHAP analysis further interpreted distinct biomarker contributions to BD prediction in the XGBC-based Model 7 (Figure 7E). The top five important factors were perianal diseases, *Erysipelatoclostridium*, fecal alanine, serum ePS(38:2), and fecal arachidonic acid. Collectively, these findings underscore the importance of integrating clinical, microbial, fecal/serum metabolomic, and imaging data into a multidimensional framework to achieve accurate BD stratification in CD patients. The superior performance of XGBC-based Model 7 justifies its selection as the optimal classifier for clinical implementation.

Discussion

Although previous studies have established associations between gut microbiota and metabolic alterations in CD, specific microbial and metabolic markers directly linked to BD in CD patients have remained elusive. Here, we effectively utilized LI to stratify patients and, for the first time, revealed the potential driving mechanisms behind damage progression in patients with high LI. Our study mapped distinct microbial and metabolic profiles associated with BD, showing that microbial dysbiosis and metabolic disturbances play critical roles in generating MRE-detectable structural lesions. Of note, by integrating the gut microbiome and fecal and serum metabolomic data with imaging features, we constructed a novel mechanism-based prediction model. This model not only underscores the pathophysiological basis of selected MRE features linked to BD but also demonstrated superior performance in distinguishing patients with BD from those without compared to models based on single data modalities.

In line with the results of previous studies, patients with BD exhibited a significant reduction in microbial dysbiosis. Specifically, beneficial genera such as *Romboutsia, Prevotella_9, Barnesiella, Fusicatenibacter*, and *Butyricicoccus* progressively decreased from HCs to NBD and BD. Their depletion may intensify mucosal inflammation and epithelial damage, fueling BD development.[22] Conversely, pathobionts such as *C. innocuum, Erysipelatoclostridium*, and *R. gnavus* were enriched in CD patients compared to HCs, consistent with their reported roles in fibrosis, barrier disruption, and inflammation.[23–25] However, *R. gnavus* and *Erysipelatoclostridium* showed a declining trend from NBD to BD, reflecting disease-related shifts in the microbial composition. These findings highlight the distinct microbial differences between BD and NBD patients, supporting the inclusion of key microbial genera in the diagnostic model to enhance its discriminatory power.

Significant shifts in both fecal and serum metabolites were also observed between patients with BD and NBD, particularly in amino acid and lipid metabolism. In fecal metabolomics, BD patients exhibited elevated levels of amino acids, organic acids, and peptides compared with NBD patients. Disruptions in aromatic amino acid metabolism may compromise the gut barrier integrity and promote inflammation.[26] The diminished levels of beneficial fatty acids, such as pimelic acid and suberic acid, may affect intestinal energy balance and anti-inflammatory processes.[27] Additionally, serum metabolomics further uncovered profound lipid metabolic disruptions in patients with BD, marked by a decline in key lipids, such as CE, Cer, SM, PC, and PE. This lipid dysregulation may indicate depletion of protective lipid reserves, leading to increased inflammation and epithelial cell death.[27] Notably, we observed significant correlations between specific bacterial genera and altered metabolite levels. Pro-inflammatory bacteria such as *Erysipelatoclostridium, R. gnavus*, and *C. innocuum* were positively associated with disrupted lipid metabolites. The preference of *C. innocuum* for lipid-rich environments and its metabolic activities may contribute to fibrosis and structural BD.[28] Moreover, beneficial bacteria such as *Fusicatenibacter* were negatively correlated with fecal amino acids. Their depletion may lead to amino acid accumulation, promoting pro-inflammatory pathways and affecting the nutritional status.[29] These metabolomic differences between patients with BD and NBD underscore the diagnostic potential of metabolic profiling, supporting the rationale for integrating metabolic factors into predictive models to improve BD stratification.

A novel finding of our study was that these microbial-metabolite interactions significantly affected MRE-detectable intestinal morphological changes. For instance, elevated *Erysipelatoclostridium* correlated with MRE features such as increased bowel wall thickness, mural T2WI hypersignal, and perienteric effusion, suggesting its pro-inflammatory role both inside and outside the gut. In contrast, the negative correlations between *Prevotella_9* and adverse MRE features, such as perianal disease and penetration, point toward its potential protective effects against severe intestinal damage and complications. Perianal disease and penetrating lesions such as fistulas and abscesses are manifestations of transmural

inflammation and are associated with a more aggressive disease course.[30] The inverse relationship with *Prevotella_9* aligns with studies suggesting that certain *Prevotella* species may have anti-inflammatory properties and support mucosal health.[31] Furthermore, reduced serum lipid metabolites (ie, PC(40:8), PC(42:10), and ePE(38:6)) were correlated with MRE-detectable features, such as penetration, indicating that lipid depletion may compromise epithelial defense mechanisms and promote deeper tissue injury.[32] These correlations emphasize that the selected MRE features not only reflect morphological changes, but also correspond to underlying microbial and metabolic disruptions, reinforcing their diagnostic relevance for BD stratification.

Leveraging the significant microbial and metabolic disturbances identified in BD patients, we developed a multi-omics prediction model that integrates gut microbiome, fecal and serum metabolites, and MRE features. This comprehensive approach allowed us to capture the complex interplay driving BD progression. The final XGBC-based Model 7, which incorporated all feature categories, demonstrated satisfactory performance in distinguishing BD from NBD patients across cohorts. This model not only improved predictive accuracy compared to models based on single data modalities but also identified key microbial and metabolic signatures driving BD. The robust performance of XGBC-based Model 7 reinforces the value of integrating diverse biological and imaging data for enhanced diagnostic precision, supporting its potential role in clinical decision-making for BD identification.

Our study had several limitations. First, our relatively modest sample size from the two centers may affect the generalizability of the findings. Future studies involving larger, multicenter cohorts across diverse geographical regions would enhance the validity of our results. Second, although we had identified significant associations of specific microbial taxa, metabolites, and imaging features with BD to develop diagnostic tool, further mechanistic studies in vitro and in vivo are necessary to elucidate the biological pathways linking these factors to BD pathogenesis, which would better establish the reliability of the optimal diagnostic tool. Third, inflammatory markers such as fecal calprotectin or clinical activity indices were not assessed due to the study's focus on cumulative structural damage; their inclusion in future studies may enable a more integrated evaluation of disease burden.

Conclusion

Our study provides novel insights into microbial and metabolic alterations associated with BD in CD patients. We identified distinct microbial signatures, including *R*. gnavus and *Erysipelatoclostridium*, and significant metabolic dysregulation in fecal and serum samples, particularly in amino acid and lipid metabolisms. These changes are closely linked to BD severity, as detected by MRE. These findings deepen our understanding of the LI as a comprehensive scoring tool for BD. Moreover, by integrating multi-omics data with imaging features, we developed a robust mechanism-based predictive model that could serve as a promising alternative for BD risk stratification. This integrated approach not only complements existing scoring systems but also paves the way for more personalized therapeutic strategies for CD.

Abbreviations

BD, bowel damage; CD, Crohn's disease; MRE, magnetic resonance enterography; LI, Lémann Index; SCFAs, short chain fatty acids; HCs, healthy controls; CDAI, Crohn's disease activity index; ESR, erythrocyte sedimentation rate; CRP, C-reactive protein; NBD, non-bowel damage; T2WI, T2-weighted imaging; DWI, diffusion weighted imaging; T1WI, T1-weighted imaging; ADC, apparent diffusion coefficient; ASV, amplicon sequence variant; OTU, operational taxonomic unit; LEfSe, linear discriminant analysis effect size; LDA, linear discriminant analysis; FDR, false discovery rate; UPLC-MS/MS, ultra-performance liquid chromatography coupled with tandem mass spectrometry; OPLS-DA, Orthogonal partial least squares discriminant analysis; VIP, variable importance; RFC, Random Forest classifier; RFE, Recursive Feature Elimination; ROC, receiver operator characteristic; AUC, area under the receiver operating characteristic curve; XGBC, eXtreme Gradient Boosting Classifier; DT, Decision Tree; RBF-SVM, Radial Basis Function Support Vector Machine; LR, Logistic Regression; KNN, K-Nearest Neighbors; SHAP, Shapley Additive exPlanations; CE, cholesteryl esters; Cer, ceramides; SM, sphingomyelins; PC, phosphatidylcholines; PE, phosphatidylethanolamines; LPC, lysophosphatidylcholines; PS, phosphatidylserines; PCoA, Principal Coordinates Analysis; PCA, Principal component analysis.

Data and Code Availability Statement

All data, analytical methods, and study materials are available from the corresponding authors (Shi-ting Feng) upon request. The raw data of fecal microbiome sequencing: Sequence Read Archive (SRA) database; accession number: PRJNA1259137; https://www.ncbi.nlm.nih.gov/sra/PRJNA1259137. The bioinformatics analysis pipelines and codes used in this study are publicly available in the GitHub repository (https://github.com/RadLLH/multiomics_CD_bowel_damage).

Ethics Approval and Consent to Participate

This prospective study was approved by the Ethics Committee of the First Affiliated Hospital of Sun Yat-sen University (No: IIT-2021[215]). All participants provided informed consent prior to inclusion in the study. This study was conducted in accordance with the ethical principles of the Declaration of Helsinki.

Acknowledgments

We would like to express our sincere gratitude to our collaborators in the Department of Gastroenterology and Department of Radiology at the Yuexiu and Nansha campuses of the First Affiliated Hospital of Sun Yat-sen University. We also extend our appreciation to all subjects who participated in this research.

Author Contributions

All authors made a significant contribution to the work reported, whether that is in the conception, study design, execution, acquisition of data, analysis and interpretation, or in all these areas; took part in drafting, revising or critically reviewing the article; gave final approval of the version to be published; have agreed on the journal to which the article has been submitted; and agree to be accountable for all aspects of the work.

Funding

This study was supported by National Natural Science Foundation of China (82270693, 82070680, 82271958, and 82471948); Guangdong Basic and Applied Basic Research Foundation (2023B1515020070, 2023A1515011097, and 2023A1515011304); Fundamental Research Funds for the Central Universities, Sun Yat-sen University (24ykqb003) and 2023 SKY Imaging Research Fund of the Chinese International Medical Foundation (Z-2014-07-2301). The funders of the study had no role in study design, data collection, data analysis, data interpretation, or writing of the report.

Disclosure

The authors report no conflicts of interest in this work.

References

1. Dolinger M, Torres J, Vermeire S. Crohn's disease. *Lancet*. 2024;403(10432):1177–1191.
2. Fiorino G, Bonifacio C, Peyrin-Biroulet L, Danese S. Preventing collateral damage in crohn's disease: the Lemann index. *J Crohns Colitis*. 2016;10(4):495–500. doi:10.1093/ecco-jcc/jjv240
3. Danese S, Fiorino G, Peyrin-Biroulet L. Early intervention in Crohn's disease: towards disease modification trials. *Gut*. 2017;66(12):2179–2187. doi:10.1136/gutjnl-2017-314519
4. Thia KT, Sandborn WJ, Harmsen WS, Zinsmeister AR, Loftus EV. Risk factors associated with progression to intestinal complications of Crohn's disease in a population-based cohort. *Gastroenterology*. 2010;139(4):1147–1155. doi:10.1053/j.gastro.2010.06.070
5. Pariente B, Mary JY, Danese S, et al. Development of the Lemann index to assess digestive tract damage in patients with crohn's disease. *Gastroenterology*. 2015;148(1):52–63. doi:10.1053/j.gastro.2014.09.015
6. Pariente B, Torres J, Burisch J, et al. Validation and update of the Lémann index to measure cumulative structural bowel damage in Crohn's disease. *Gastroenterology*. 2021;161(3):853–864e813. doi:10.1053/j.gastro.2021.05.049
7. Fiorino G, Bonifacio C, Allocca M, et al. Bowel damage as assessed by the Lemann index is reversible on anti-TNF therapy for Crohn's disease. *Journal of Crohn's and Colitis*. 2015;9(8):633–639. doi:10.1093/ecco-jcc/jjv080
8. Rimola J, Ordas I, Rodriguez S, et al. Magnetic resonance imaging for evaluation of Crohn's disease. *Inflamm Bowel Dis*. 2011;17(8):1759–1768. doi:10.1002/ibd.21551
9. Hanzel J, Jairath V, Ma C, et al. Responsiveness of magnetic resonance enterography indices for evaluation of luminal disease activity in Crohn's disease. *Clin Gastroenterol Hepatol*. 2022;20(11):2598–2606. doi:10.1016/j.cgh.2022.01.055
10. Li XH, Sun CH, Mao R, et al. Diffusion-weighted MRI enables to accurately grade inflammatory activity in patients of ileocolonic Crohn's disease: results from an observational study. *Inflamm Bowel Dis*. 2017;23(2):244–253.

11. Pascal V, Pozuelo M, Borruel N, et al. A microbial signature for Crohn's disease. *Gut*. 2017;66(5):813–822.
12. Lavelle A, Sokol H. Gut microbiota-derived metabolites as key actors in inflammatory bowel disease. *Nat Rev Gastroenterol Hepatol*. 2020;17(4):223–237.
13. Schirmer M, Garner A, Vlamakis H, Xavier RJ. Microbial genes and pathways in inflammatory bowel disease. *Nat Rev Microbiol*. 2019;17(8):497–511. doi:10.1038/s41579-019-0213-6
14. Franzosa EA, Sirota-Madi A, Avila-Pacheco J, et al. Gut microbiome structure and metabolic activity in inflammatory bowel disease. *Nat Microbiol*. 2019;4(2):293–305. doi:10.1038/s41564-018-0306-4
15. Lee JWJ, Plichta D, Hogstrom L, et al. Multi-omics reveal microbial determinants impacting responses to biologic therapies in inflammatory bowel disease. *Cell Host Microbe*. 2021;29(8):1294–1304e1294. doi:10.1016/j.chom.2021.06.019
16. Li X, Hu S, Shen X, et al. Multiomics reveals microbial metabolites as key actors in intestinal fibrosis in Crohn's disease. *EMBO Mol Med*. 2024;16(10):2427–2449. doi:10.1038/s44321-024-00129-8
17. Alam MT, Amos GCA, Murphy ARJ, Murch S, Wellington EMH, Arasaradnam RP. Microbial imbalance in inflammatory bowel disease patients at different taxonomic levels. *Gut Pathog*. 2020;12(1):1. doi:10.1186/s13099-019-0341-6
18. Manandhar M, Cronan JE. Pimelic acid, the first precursor of the Bacillus subtilis biotin synthesis pathway, exists as the free acid and is assembled by fatty acid synthesis. *Mol Microbiol*. 2017;104(4):595–607. doi:10.1111/mmi.13648
19. Das UN. Arachidonic acid in health and disease with focus on hypertension and diabetes mellitus: a review. *J Adv Res*. 2018;11:43–55. doi:10.1016/j.jare.2018.01.002
20. Metherel AH, Lacombe RJS, Chouinard-Watkins R, Hopperton KE, Bazinet RP. Complete assessment of whole-body n-3 and n-6 PUFA synthesis-secretion kinetics and DHA turnover in a rodent model. *J Lipid Res*. 2018;59(2):357–367. doi:10.1194/jlr.M081380
21. Ha CWY, Martin A, Sepich-Poore GD, et al. Translocation of viable gut microbiota to mesenteric adipose drives formation of creeping fat in humans. *Cell*. 2020;183(3):666–683e617. doi:10.1016/j.cell.2020.09.009
22. Recharla N, Geesala R, Shi XZ. Gut microbial metabolite butyrate and its therapeutic role in inflammatory bowel disease: a literature review. *Nutrients*. 2023;15(10):10. doi:10.3390/nu15102275
23. Ning LJ, Zhou YL, Sun H, et al. Microbiome and metabolome features in inflammatory bowel disease via multi-omics integration analyses across cohorts. *Nat Commun*. 2023;14(1):1. doi:10.1038/s41467-023-42788-0
24. Hall AB, Yassour M, Sauk J, et al. A novel Ruminococcus gnavus clade enriched in inflammatory bowel disease patients. *Genome Med*. 2017;9(1):103. doi:10.1186/s13073-017-0490-5
25. Le PH, Chiu CT, Yeh PJ, Pan YB, Chiu CH. Clostridium innocuum infection in hospitalised patients with inflammatory bowel disease. *J Infect*. 2022;84(3):337–342. doi:10.1016/j.jinf.2021.12.031
26. Agus A, Planchais J, Sokol H. Gut microbiota regulation of tryptophan metabolism in health and disease. *Cell Host Microbe*. 2018;23(6):716–724. doi:10.1016/j.chom.2018.05.003
27. Dias VC, Fung E, Snyder FF, Carter RJ, Parsons HG. Effects of medium-chain triglyceride feeding on energy balance in adult humans. *Metabolism*. 1990;39(9):887–891. doi:10.1016/0026-0495(90)90295-N
28. Wu HY, Kuo CJ, Chou CH, et al. Clostridium innocuum, an emerging pathogen that induces lipid raft-mediated cytotoxicity. *Virulence*. 2023;14(1):2265048. doi:10.1080/21505594.2023.2265048
29. Bourgonje AR, Feelisch M, Faber KN, Pasch A, Dijkstra G, van Goor H. Oxidative stress and redox-modulating therapeutics in inflammatory bowel disease. *Trends Mol Med*. 2020;26(11):1034–1046. doi:10.1016/j.molmed.2020.06.006
30. Meng XF, Lin QY, Yin HL, Li ZQ. Magnetic resonance imaging for evaluation of bowel inflammation and disease activity in Crohn's disease: a systematic review and meta-analysis. *Gastroenterol Hepatol*. 2023;46(5):336–349. doi:10.1016/j.gastrohep.2022.10.004
31. Kovatcheva-Datchary P, Nilsson A, Akrami R, et al. Dietary fiber-induced improvement in glucose metabolism is associated with increased abundance of prevotella. *Cell Metab*. 2015;22(6):971–982. doi:10.1016/j.cmet.2015.10.001
32. Ferru-Clement R, Boucher G, Forest A, et al. Serum lipidomic screen identifies key metabolites, pathways, and disease classifiers in Crohn's disease. *Inflamm Bowel Dis*. 2023;29(7):1024–1037. doi:10.1093/ibd/izac281